Inorganic Chemistry

Article

pubs.acs.org/IC

Syntheses, Structures, and Luminescent Properties of Dipyridylamine-Functionalized Anthracene and Its Complexes

Runyu Tan,[†] Zhi-Bin Wang,[‡] Yu Li,[†] Daniel J. Kozera,[†] Zheng-Hong Lu,[‡] and Datong Song*[,†]

[†]Davenport Chemical Research Laboratories, Department of Chemistry, University of Toronto, 80 St. George Street, Toronto, Ontario, Canada M5S 3H6

[‡]Department of Materials Science and Engineering, University of Toronto, 184 College Street, Toronto, Ontario, Canada M5S 3E4

Supporting Information

ABSTRACT: A novel multidentate ligand with 2,2′-dipyridylamine functionalities, 1,8-bis[4-(2,2′-dipyridylamino)-phenylacetylenyl]anthracene (**1**), has been synthesized through a double Sonogashira coupling reaction and characterized by NMR spectroscopic, elemental, and X-ray diffraction analyses. Compound **1** can bind to either one metal center as a tetradentate ligand or two metal centers as a double-bidentate ligand. In the double-bidentate mode, the distance between the two metal centers may vary significantly. Compound **1** displays bright blue luminescence in the solid state and in solution with a quantum efficiency of 64% relative to 9,10-diphenylanthracene. While the dirhodium complex of **1** shows no luminescence, the two zinc complexes of **1** display blue luminescence with quantum efficiencies slightly lower than that of **1**. Organic light-emitting devices (OLEDs) using **1** as the emitter show a maximum current efficiency of 7 cd/A.

INTRODUCTION

Because of their photophysical properties, luminescent organic compounds have found use in many fields such as sensing,[1−7] imaging,[8−10] and solid-state lighting.[11−13] Luminescent organic compounds with metal binding ability are even more interesting, because metal binding would improve the rigidity of the molecule and in turn reduce the luminescence quenching caused by thermal vibration. In addition, metal binding may change the stability of the molecule. Moreover, heavy metals such as Pt and Ir would facilitate intersystem crossing and therefore make phosphorescence emission practically useful in organic light-emitting devices (OLEDs).[14−18] Our group is interested in luminescent organic molecules with versatile metal binding modes, because different metal binding modes are associated with various symmetries and orbital energy levels of the molecule and affect the luminescent properties. This should allow us to investigate the photophysical properties of various metal complexes of the organic ligand and to gain an understanding of how the ligand geometry change enforced by the metal center would alter the photophysical properties.

Our recent ligand design incorporates two luminescent metal binding units and a luminescent spacer to provide the required separation between two potential binding sites. To achieve the desired degree of flexibility of the binucleating ligand, instead of tethering two metal binding groups directly onto a rigid anthracene moiety,[19−30] we install them onto a U-shaped linker that consists of two phenylacetylene moieties attached to the 1,8-positions of an anthracene unit. We reason that by increasing the length of the linker a certain degree of flexibility could be realized. We chose 2,2′-dipyridylamine (DPA) as the metal binding unit in our ligand design for its versatile metal binding modes. Furthermore, DPA-functionalized ligands and metal complexes have been found to be highly luminescent and hence have been used as luminescent sensors and in OLEDs.[31,32] For example, the Ye group has reported a tetrakis(dipyridylamine)-functionalized zinc porphyrin ligand that can sense Cu^{2+} selectively by fluorescence quenching upon binding of Cu^{2+} through the DPA moieties.[31] Wang and co-workers have studied DPA-containing molecules extensively.[33−39] They reported a series of linear and starburst-shaped molecules that utilize DPA moieties to accommodate

Received: August 12, 2011
Published: June 11, 2012

Scheme 1. Synthesis of Ligand 1

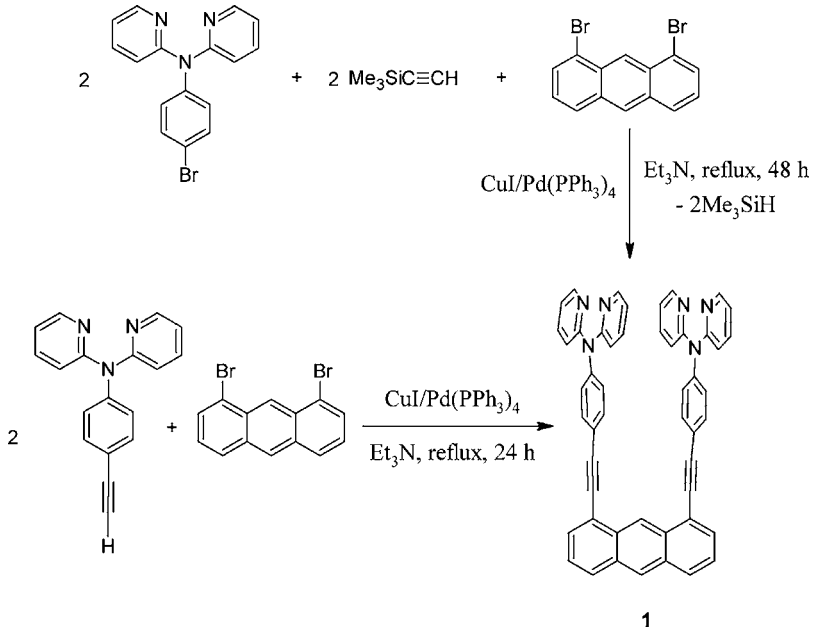

different metals. In these molecules, phenyl, silole, or triazine groups are used as linkers. Some of these compounds are promising candidates as emitters or electron transport materials in OLEDs. In this paper, we report our effort to synthesize a U-shaped ligand with DPA functional groups and the study of its versatile coordination behavior caused by the less rigid linker group as well as the luminescent properties of such a ligand and its metal complexes.

RESULTS AND DISCUSSION

Synthesis of the Ligand 1. Ligand **1** can be synthesized in good yield through a Sonogashira coupling reaction of 1,8-dibromoanthracene and 4-(2,2′-dipyridylamino)-phenylacetylene using $PdCl_2(PPh_3)_2$/CuI as catalyst and Et_3N as solvent (Scheme 1).[40] Alternatively, **1** can be synthesized via a multicomponent one-pot reaction from 1,8-dibromoanthracene, (trimethylsilyl)acetylene, and 4-(2,2′-dipyridylamino)-phenyl bromide under similar conditions. ^1H and ^{13}C NMR spectra of **1** indicated a symmetric structure in solution with only one set of DPA resonance peaks. The solid-state structure of **1** was unambiguously confirmed by X-ray crystallography. As shown in Figure 1, the two phenylethynyl linkers are linear and parallel to each other.

The ground-state geometry of **1** was fully optimized using the crystal structure as the starting geometry. The diagrams of the frontier orbitals and their energy levels are shown in Figure 2. No symmetry restraint was imposed on the molecule, and the optimized structure is slightly unsymmetrical, in contrast to the symmetrical NMR spectrum, as a result of free rotation in solution. Consequently, the MOs have slightly uneven contribution from the two branches of the molecule. As shown in Figure 2, the main contributor to HOMO-1 (−0.207 82 hartree) is the filled p orbital of the tertiary nitrogen of DPA, the HOMO (−0.199 29 hartree) has significant contributions from the p orbital of the tertiary nitrogen of DPA and the π orbital of anthracene and phenylethynyl moieties, the LUMO (−0.090 29 hartree) has mainly the π^* character of the anthracene moiety, and the LUMO+1 (−0.065 56 hartree) shows the π^* character of the U-shaped spacer.

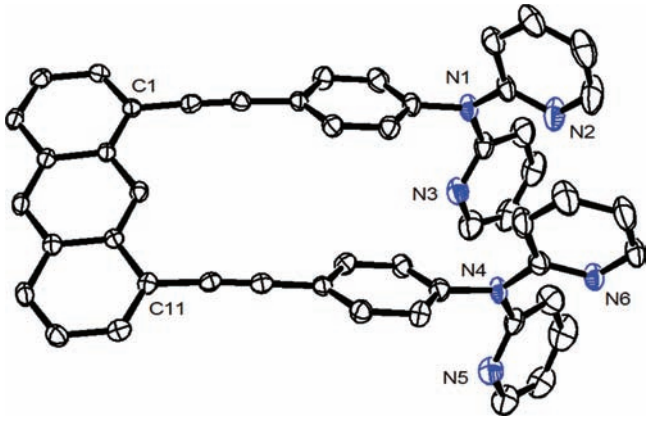

Figure 1. Molecular structure of **1** with thermal ellipsoids plotted at the 50% probability level. Hydrogen atoms are omitted for clarity.

Coordination Chemistry of 1. One of the vital features of compound **1** is that two DPA moieties are juxtaposed by the U-shaped linker group with the separation distance of two tertiary amine nitrogen atoms being ∼5 Å. As a result, they could potentially accommodate two metals in close proximity. The distances between the two metal centers may vary with different auxiliary ligands as well as the coordination geometry of the metal center. When **1** is treated with 2 equiv of $[Rh(COD)(CH_3CN)_2]BF_4$ in THF (Scheme 2, left), the quantitative formation of the product **2a** can be observed. The solid-state structure of **2a** was confirmed by X-ray crystallography. As shown in Figure 3, **2a** consists of two Rh(COD) moieties per ligand **1**. Each rhodium center adopts a square-planar geometry and is coordinated with two pyridine nitrogen donor atoms of the DPA moiety and two CC double bonds of COD in a cis,cis fashion. To accommodate this geometry, the dihedral angles between the two pyridine rings within one DPA moiety are 58.44 and 67.92°, respectively. The two phenylethynyl linkers deviate slightly from a linear geometry and bend away from each other, creating a very large Rh−Rh distance (12.306(4) Å).

dx.doi.org/10.1021/ic201757r | Inorg. Chem. 2012, 51, 7039−7049

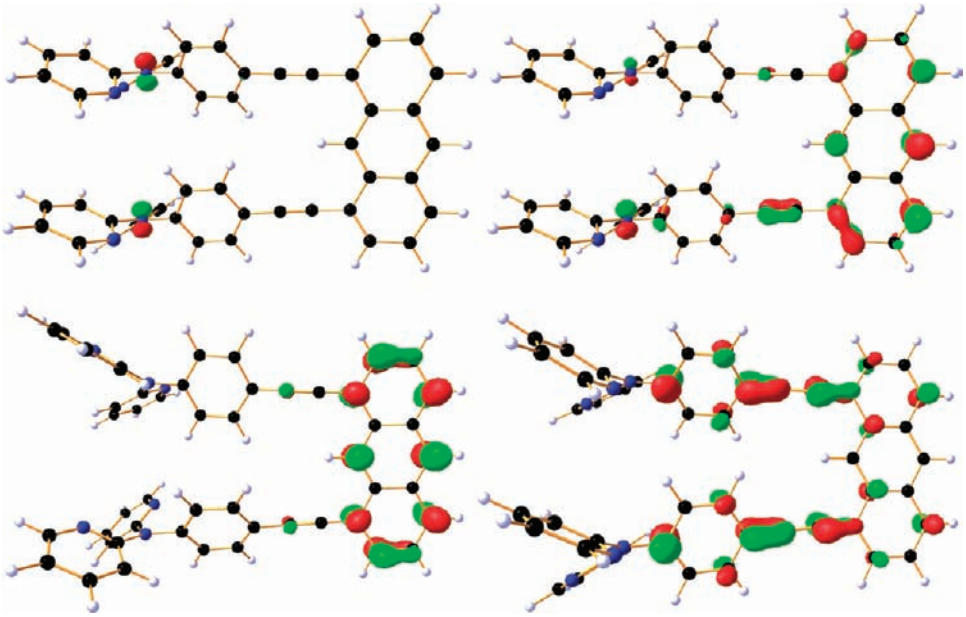

Figure 2. HOMO-1 (top left), HOMO (top right), LUMO (bottom left), and LUMO+1 (bottom right) diagrams of compound **1**.

Scheme 2. Synthesis of 2

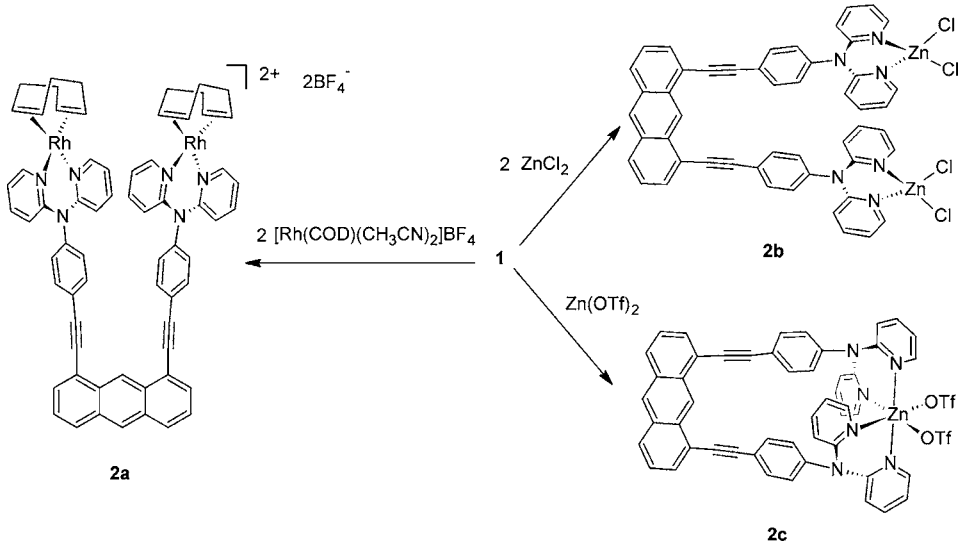

We next sought to explore the reactivity of ligand **1** toward metals with other coordination geometries. When **1** was treated with 2 equiv of $ZnCl_2$ in THF (Scheme 2, top right), quantitative formation of the new species **2b** was observed in both ^1H and ^{13}C NMR spectra. Although the ^1H resonances of **2b** shifted appreciably compared to those of **1**, the ^{13}C resonances are similar to those of **1**. X-ray crystallography showed that **2b** is a dinuclear zinc complex. It crystallized in the orthorhombic space group *Pnna* and has a crystallographically imposed 2-fold symmetry. As shown in Figure 4, each zinc center adopts a tetrahedral geometry, with two pyridine nitrogen atoms within one DPA group and two chlorides occupying the four coordination sites. The dihedral angle between the two pyridine rings within one DPA is 25.54°, which is much smaller than those in **2a**. There are $\pi-\pi$ stacking interactions between two of the pyridine rings that are close to the C_2 axis with a short contact distance of ~3.47 Å. The distance between the two metal centers (7.723 Å) is much shorter than that in **2a**. Interestingly, molecules of **2b** stack along the *b* axis in the crystal lattice with large 1-D solvent channels in between (Figure 5). The framework is held together by the weak intermolecular hydrogen-bonding interactions between the chlorides and aromatic protons as well as the weak intermolecular head-to-edge interactions between the phenyl C−H bonds and the anthracene moiety next to it. The solvent molecules in the channels were not fully located, which, however, appeared to be unimportant, since the same framework can be obtained by crystallizing **2b** in different solvents such as DCM and THF/CH_3CN (see **2b′** in the Supporting Information). The persistence of this framework with extraordinarily large channels opens up a possibility of utilizing this material for sensing applications and size-selective catalysis.

To shorten the distance between the two Zn(II) centers, we sought bridging anionic ligands to tie the two metal centers together. Inspired by the Zn(II)-containing phosphotriesterase

dx.doi.org/10.1021/ic201757r | *Inorg. Chem.* 2012, 51, 7039−7049

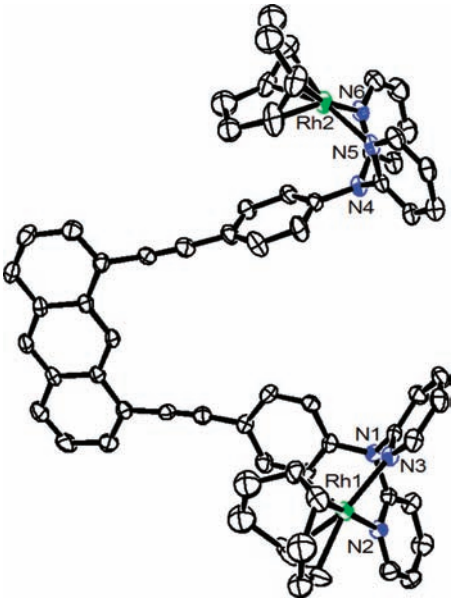

Figure 3. Molecular structure of **2a** with thermal ellipsoids plotted at the 50% probability level. All hydrogen atoms and BF_4^- counterions are omitted for clarity.

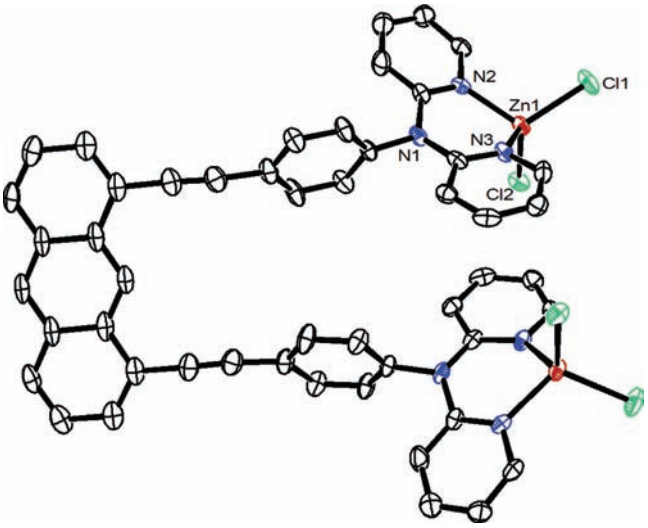

Figure 4. Molecular structure of **2b** with thermal ellipsoids plotted at the 50% probability level. All hydrogen atoms are omitted for clarity.

whose active site comprises two Zn^{2+} ions bridged by carboxylate ligands with a short metal−metal distance, we tried to introduce acetates and triflates into the construction of dizinc complexes. ^1H and ^{13}C NMR spectra of the 1:2 mixture of **1** and $Zn(OAc)_2$ are very similar to those of the free ligand, suggesting that **1** does not bind to $Zn(OAc)_2$ very well. Attempts to crystallize the reaction mixture of **1** and $Zn(OAc)_2$ always resulted in the isolation of free ligand **1**. However, when **1** was treated with 2 equiv of $Zn(OTf)_2$, significant chemical shift changes were observed in both the ^1H and ^{13}C NMR spectra in comparison to those of the free ligand. Recrystallization of the reaction mixture yielded pale yellow crystals which are suitable for X-ray crystallographic analyses. Instead of a dizinc complex, the mononuclear zinc complex **2c** was obtained, despite the fact that 2 equiv of $Zn(OTf)_2$ was used (Scheme 2, bottom right). As shown in Figure 6, the molecule **2c** has a crystallographically imposed C_2 symmetry and each zinc center adopts an octahedral geometry, with four pyridine nitrogen atoms occupying four coordination sites and two triflate ligands occupying the remaining two in a cis fashion. The dihedral angle between the two pyridine rings of the same DPA moiety is 41.54°, much larger than that in **2b**. The distance between the two amino nitrogen atoms is 4.474(5) Å, drastically shorter than that in **2a** (8.190(5) Å) or **2b** (6.501(4) Å), demonstrating the flexibility of the U-shaped linker group. In fact, the distance between the two amino nitrogen atoms in **2c** is even shorter than that in the free ligand **1** (5.020(3) Å): i.e., the two branches of the U-shaped linker are bending inward in **2c**, in contrast to the outward bending conformation in **2a**,**b**. Alternatively, **2c** can be synthesized by treating **1** with 1 equiv of $Zn(OTf)_2$. Interestingly, the ^1H NMR spectrum of the 1:2 mixture of **1** and $Zn(OTf)_2$ is identical with that of **2c** and no further change was observed with addition of an excess amount of $Zn(OTf)_2$. Even the slow addition of ligand **1** solution into a $Zn(OTf)_2$ solution only produced **2c** without forming any dinuclear metal complexes, in contrast to the literature examples of triflate-bridged dizinc complexes.[41,42]

Photophysical Properties. The UV−vis spectra of **1** in various solvents show similar shapes: two intense absorption bands in the UV region at 250−280 and 280−370 nm and a weaker vibrational progression band in the region of 370−450 nm (Figure 7). The band at 280−370 nm could be assigned to $\pi-\pi^*$ and n−-π^* electronic transitions of the phenylalkynyl and dipyridylamine groups.[43] The bands at 250−280 and 370−450 nm are characteristic for the anthracene moiety.[44] In methanol, while the characteristic anthracene bands remain in place, the band at 280−370 nm split into a peak at 282 nm and a shoulder at 310 nm. Such a split could be attributed to the stabilization of the tertiary nitrogen lone pair through hydrogen bonding with MeOH, which shifts the n−π^* band to the higher energy region. On irradiation with UV light, **1** emits bright blue light in solution with a quantum efficiency of 0.65 relative to 9,10-diphenylanthracene. While the lowest energy absorption band of **1** in various solvents shifts from short to long wavelength according to the sequence MeOH < CH_3CN < THF < DCM ≈ DMF < DMSO, the emission band of **1** in these solvents shifts from short to long wavelength according to the slightly different sequence MeOH < DCM ≈ THF < CH_3CN ≈ DMF < DMSO (note the position change of CH_3CN in the series). This difference is not yet fully understood. The emission band shift of **1** appears to correspond to the polarity of the solvent: i.e. a red shift with increasing solvent polarity in aprotic solvents (Figure 8), indicating a polarized excited state.[45,46] In methanol, the emission band of **1** exhibits a blue shift compared to those in dichloromethane and THF, which are less polar than methanol.[47] This shift is presumably due to the stabilization of the tertiary amine nitrogen lone pairs, a contributor of the HOMOs, through hydrogen-bonding interactions with the solvent molecules.[48] While **2a** does not exhibit noticeable emission in solution, the emission spectrum of **2b** in DCM is very similar to that of **1** in the same solvent (Figure 9). The emission spectrum of **2c** in DCM features two maxima at 430 and 457 nm, similar to that of **1** in hexanes. Compounds **2b**,**c** in DCM show photoluminescence quantum efficiencies of 0.57 and 0.54 (relative to 9,10-diphenylanthracene), respectively, lower than that of the free ligand **1**.

Electroluminescent Properties of 1. The bright blue luminescence of **1** in the solid state prompted us to explore its electroluminescent properties. We fabricated OLEDs using **1** as

dx.doi.org/10.1021/ic201757r | Inorg. Chem. 2012, 51, 7039−7049

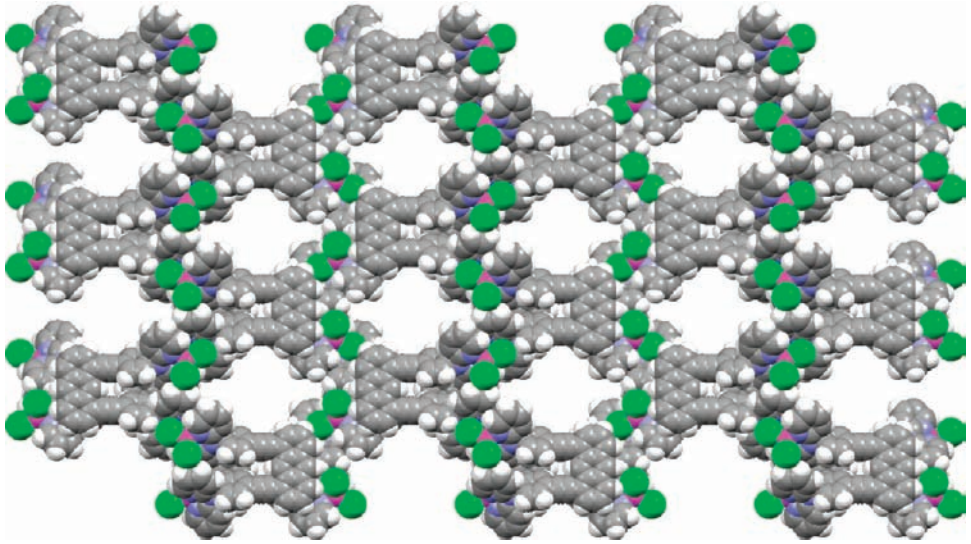

Figure 5. Space-filling model showing channels in the lattice of **2b** along the *b* axis. All solvents are removed for clarity.

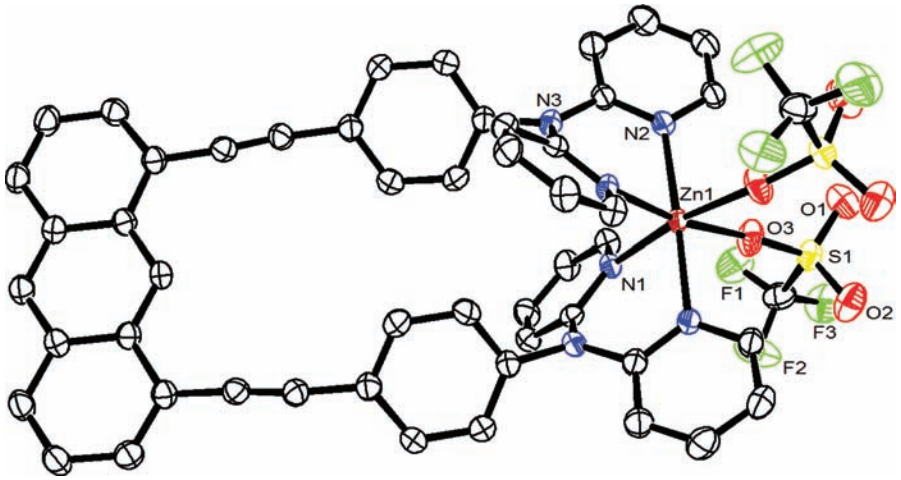

Figure 6. Molecular structure of **2c** with thermal ellipsoids plotted at the 50% probability level. All hydrogen atoms are omitted for clarity.

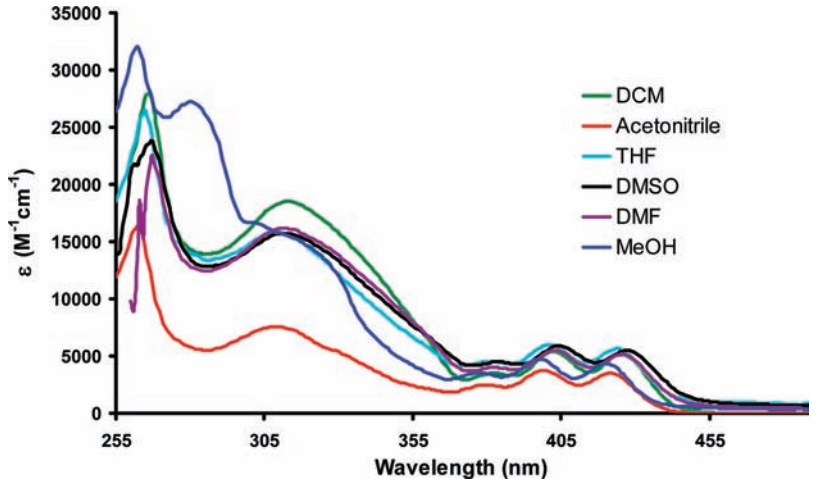

Figure 7. Absorption spectra of compound **1** in various solvents (~10^{-5} M).

emitter with the device structure shown schematically in Figure 10, where 4,4′-bis(carbazol-9-yl)biphenyl (CBP) and 2,2′,2″-(1,3,5-benzenetriyl)tris(1-phenyl-1*H*-benzimidazole) (TPBi) are selected as the hole transport layer (HTL) and electron transport layer (ETL), respectively. The emitter is either a neat film of **1** or **1** doped in different host molecules: i.e., *N*,*N*′-diphenyl-*N*,*N*′-bis(1-naphthyl)-1,1′-biphenyl-4,4′-diamine (*α*-NPD), CBP, and TPBi. It has been demonstrated that CBP

dx.doi.org/10.1021/ic201757r | *Inorg. Chem.* 2012, 51, 7039–7049

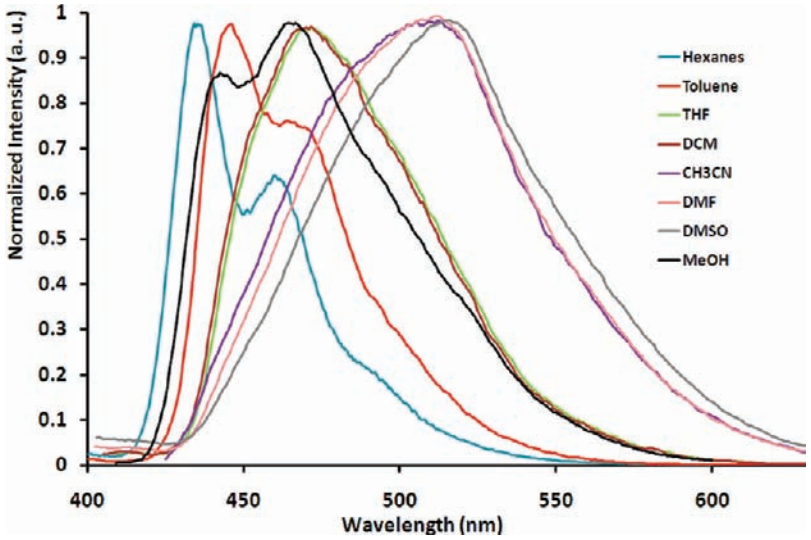

Figure 8. Emission spectra of compound **1** in various solvents ($\sim 10^{-5}$ M) using 400 nm excitation wavelength.

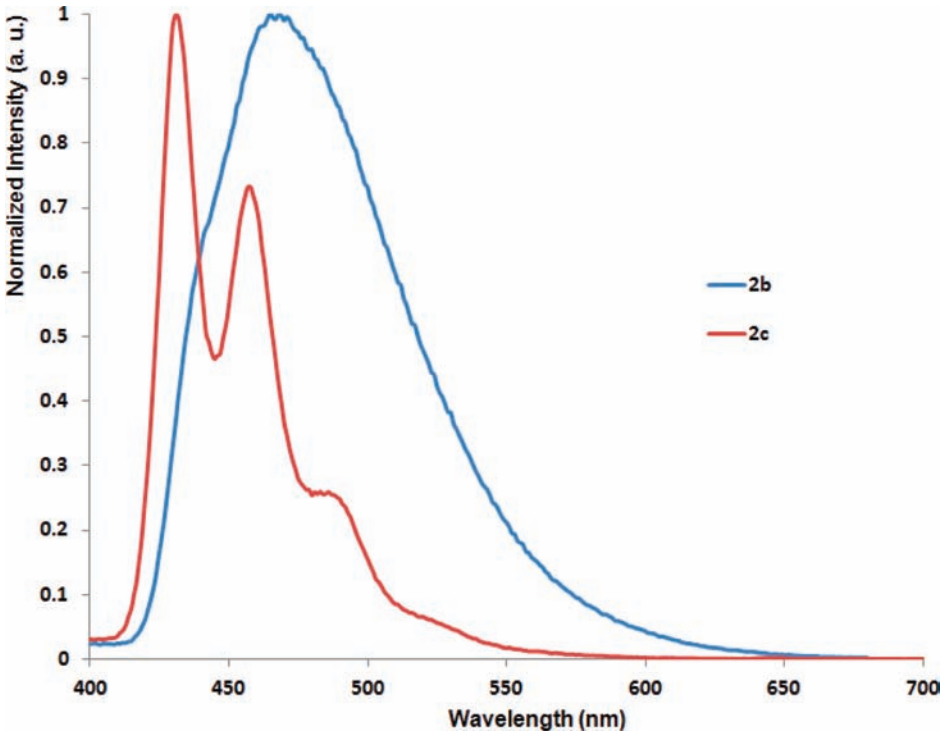

Figure 9. Emission spectra of compounds **2b**,**c** in dichloromethane ($\sim 10^{-5}$ M) using 400 nm excitation wavelength.

and TPBi can reduce the accumulation of carriers at different organic/organic interfaces (such as the HTL/emission layer (EML) and EML/ETL) and thus enhance the device performance.[49−51] The OLED device performances of **1** doped in different hosts with 1 wt % doping concentration as well as a neat film of **1** as EML (indicated as neat film) are summarized in Figure 11. Figure 11a shows the EL spectrum of different devices and the PL spectrum of **1** in the solid state. The emission band of the PL spectrum has a maximum at 478 nm, while the emission bands of EL spectra depend on the host molecules. When TPBi is used as the host in the EML, there is also a shoulder at 399 nm in the EL spectrum as a result of the emission from TPBi (see the PL spectrum of TPBi from Figure 11f).

The benefit of using a guest−host system is that the charge transport can be separated from the emission process.[52] Figure 11f shows the solid-state PL spectrum of different hosts in comparison with the absorption spectrum of **1** that is shown in Figure 3. The considerable overlap of the PL emission spectrum of CBP and TPBi with the absorption spectrum of **1** suggests effective Förster and/or Dexter energy transfer from the host to the dopant: e.g., from the singlet level of TPBi to the single level of **1**. The greatly decreased overlap of the PL spectrum of α-NPD with the absorption spectrum of **1** is in good agreement with the lower efficiency of the α-NPD device: i.e., the energy transfer between the α-NPD and **1** is not as effective. Although the PL spectra of TPBi and CBP have a similar overlap with the absorption spectrum of **1**, both the

dx.doi.org/10.1021/ic201757r | *Inorg. Chem.* 2012, 51, 7039−7049

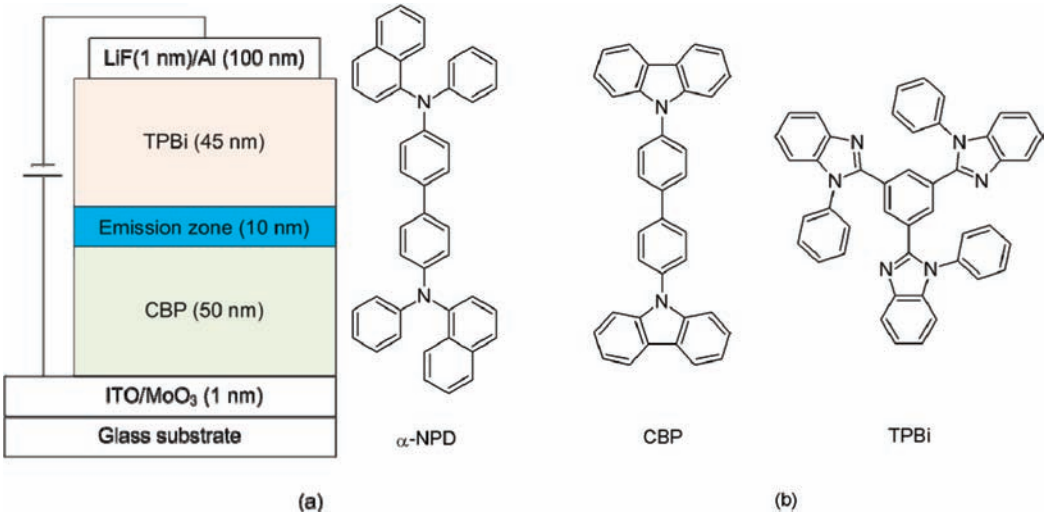

Figure 10. (a) Schematic diagram of the trilayer OLED structure with the emission zone (neat **1**, **1** doped with CBP, or **1** doped with TPBi) sandwiched between CBP and TPBi. (b) Structures of α-NPD, CBP, and TPBi.

current efficiency and external quantum efficiency (EQE) of the TPBi device are higher than those of the CBP device over a broad range of luminance (Figure 11b,c). This may be attributed to the difference of the electrical properties (i.e., mobility and energy level alignment at organic/organic interface) between the **1**-doped TPBi and **1**-doped CBP, which can be seen from the significantly lower turn-on voltage (>10 V at 10 mA/cm^2) of the TPBi device in comparison to that of the CBP device (see Figure 11d,e).

As mentioned above, in the TPBi device emission from TPBi was observed, which indicates that there is some loss of exciton in the device with a TPBi host due to the leakage current. To reduce the leakage current and the emission from TPBi, we also fabricated devices with higher doping concentrations of **1** into TPBi, i.e., 5 and 10 wt %. The current efficiency, power efficiency, EQE, and EL spectra of the devices with different doping concentrations are shown in Figure 12. Among the three doping concentrations, a higher doping concentration gives higher current efficiency, reaching ~7 cd/A at 1 cd/m^2. However, there is no significant improvement in the EQE when the doping concentration is increased from 5% to 10%. The highest EQE at 1000 cd/m^2 (i.e., ~1.5%), a typical brightness for display applications, was achieved with 5% doping and the corresponding current efficiency and power efficiency were 2.2 cd/A and 1.2 lm/W, respectively. The peak EQE value of this device was as high as ~4.0% at low luminance (1 cd/m^2), which is among the highest EQE values for fluorescent blue OLEDs reported in the literature.[53] Also, as the doping concentration increases, less emission from TPBi can be observed. The shape of the EL spectrum at higher doping concentration is similar to that of the PL spectrum of **1**.

CONCLUSION

In conclusion, a novel U-shaped multidentate ligand has been designed and synthesized. Due to the flexibility of the ligand, this ligand can act either as a double-bidentate ligand, bringing two metals in close proximity, or as a tetradentate ligand, coordinating to one metal via four nitrogen donor atoms. Compound **1** and its zinc complexes **2b**,**c** display bright blue luminescence with high PL quantum efficiencies. The application of **1** as a blue emitter in OLED with current efficiency as high as 7 cd/A has been successfully demonstrated at low luminance. Such a current efficiency is much higher than those of known OLEDs with DPA-derivative-based emitters in the literature.[33,36] The external quantum efficiency of our device is among the best of the blue fluorescent OLEDs reported in the literature.

EXPERIMENTAL SECTION

General Considerations. All preparations and manipulations were performed under nitrogen using standard Schlenk techniques or in a nitrogen atmosphere glovebox from MBraun. Unless otherwise stated, all reagents were purchased from commercial sources and used without further purification. 1,8-Dibromoanthracene,[54] (4-(2,2′-dipyridylamino)phenyl)acetylene,[55] and [Rh(COD)(CH$_3$CN)$_2$]BF$_4$[56] were synthesized according to literature procedures. ^{1}H, ^{13}C{^{1}H}, and ^{19}F spectra were recorded on a Varian 400 or a Bruker Avance 400 spectrometer. Chemical shifts were referenced relative to the solvent's residual signals but are reported relative to Me$_4$Si. The UV−vis spectra were measured using an Agilent 8453 UV−visible spectrophotometer. The solution photoluminescence (PL) spectra were measured using a JY HORIBA Fluorolog-3 spectrofluorometer or a Perkin-Elmer LS-50B luminescence spectrophotometer, while the solid-state PL spectra were measured using a Perkin-Elmer LS55 fluorescence spectrometer. Elemental analyses were performed on a PE 2400 C/H/N/S analyzer at the Analest of our Chemistry Department.

Synthesis of 1,8-Bis[4-(2,2′-dipyridylamino)-phenylacetylenyl]anthracene (1). To a mixture of (4-(2,2′-dipyridylamino)phenyl)acetylene (466 mg, 1.69 mmol), 1,8-dibromoanthracene (264 mg, 0.787 mmol), Pd(PPh$_3$)$_4$ (91 mg, 0.08 mmol), and CuI (15 mg, 0.08 mmol), was added 20 mL of degassed Et$_3$N. The mixture was then refluxed for 24 h. The resulting yellow suspension was cooled to ambient temperature, and the solvent was removed under reduced pressure. The residue was subjected to silica gel column chromatography using THF/hexanes (1/1 volume ratio) as eluent to yield the product as a yellow powder (71% yield). *Alternative method*: to a mixture of 4-(2,2′-dipyridylamino)phenyl bromide (639 mg, 1.96 mmol), 1,8-dibromoanthracene (264 mg, 0.787 mmol), Pd(PPh$_3$)$_4$ (91 mg, 0.08 mmol), and CuI (15 mg, 0.08 mmol) was added a mixture of degassed Et$_3$N (20 mL) and Me$_3$SiCCH (0.28 mL, 1.96 mmol). The resulting mixture was then refluxed for 48 h. The workup procedure was the same as above (20% yield). ^{1}H NMR (CDCl$_3$, 400 MHz, 25 °C): δ 9.60 (s, 1H), 8.47 (s, 1H), 8.26 (d, J = 4.0 Hz, 4H), 8.02 (d, J = 4.0 Hz, 2H), 7.81 (d, J = 8.0 Hz, 2H), 7.63 (d, J = 4.0 Hz, 4H), 7.50−7.46 (m, 6H), 7.04 (d, J = 8.0 Hz, 4H), 6.91 (d, J = 12.0 Hz, 4H), 6.88 (dd, J = 8.0 Hz, J = 4.0 Hz, 4H). ^{13}C{^{1}H} NMR (CDCl$_3$, 100 MHz, 25 °C): δ 171.0, 157.6, 148.5,

dx.doi.org/10.1021/ic201757r | Inorg. Chem. 2012, 51, 7039−7049

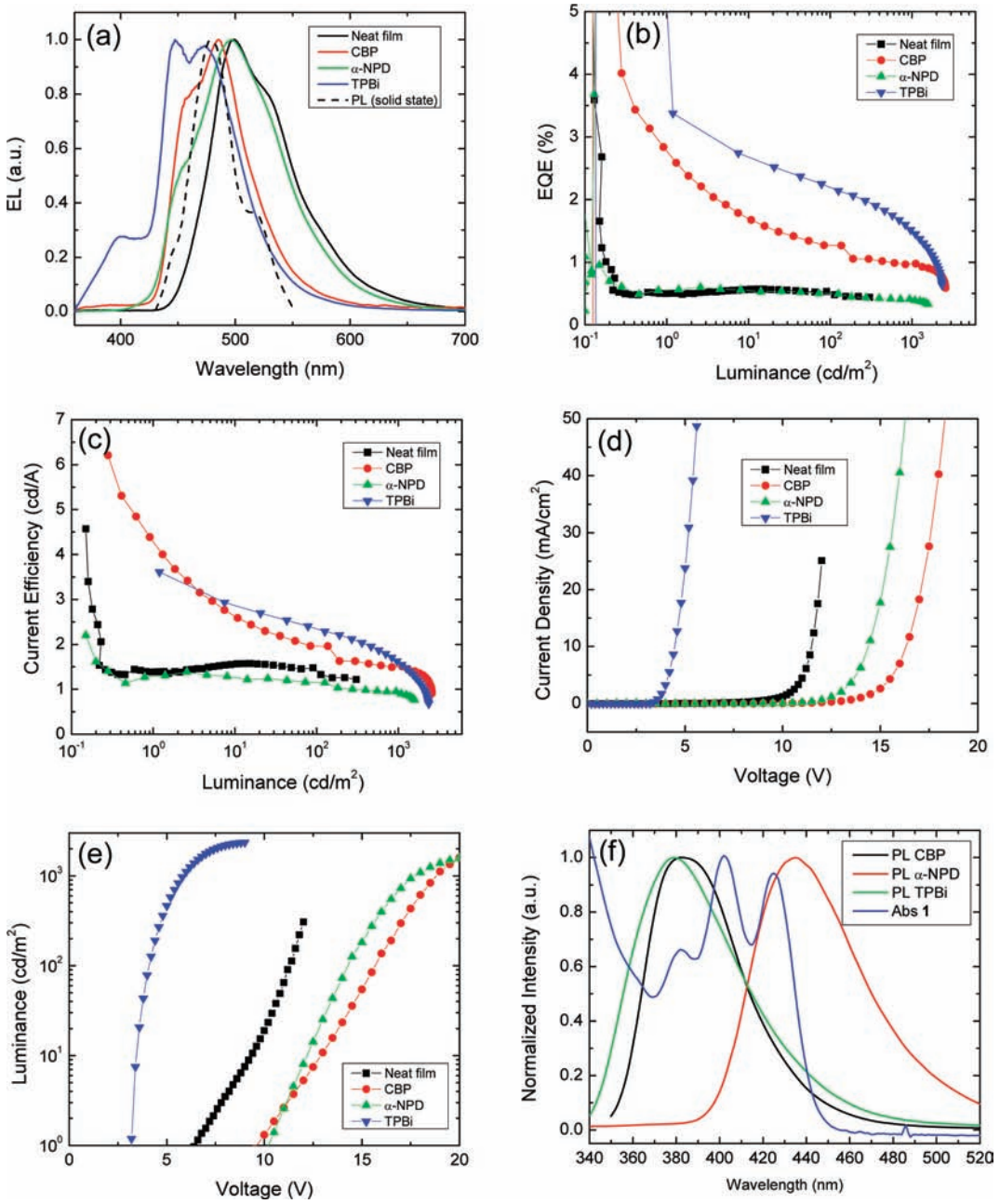

Figure 11. (a) Normalized EL spectra, (b) current efficiency as a function of luminance, (c) current–voltage characteristics (*IV*), and (d) luminance–voltage characteristics (*LV*) of OLED devices with **1** in different hosts as EML. The performance of pure **1** film as the EML is also shown and indicated as the neat film. (f) Solid-state PL spectra of different hosts in comparison with the absorption spectrum of **1** that is shown in Figure 3.

145.0, 137.6, 133.1, 131.6, 131.4, 130.7, 128.8, 126.7, 125.2, 124.1, 121.7, 120.1, 118.5, 117.1, 94.77, 87.94. Anal. Calcd for $C_{50}H_{32}N_6 \cdot {}^1/_3CHCl_3$: C, 79.68; H, 4.62; N, 11.07. Found: C, 79.90; H, 4.31; N, 11.11.

Synthesis of $[Rh_2(1)(COD)_2](BF_4)_2$ (2a). A mixture of **1** (7.2 mg, 0.01 mmol) and $[Rh(COD)(CH_3CN)_2]BF_4$ (7.6 mg, 0.02 mmol) was dissolved in 4 mL of CH_2Cl_2, and the solution was stirred for 2 h. The solvent was removed in vacuo, and the residue was recrytallized in dichloromethane/hexanes to yield the product as a pale yellow crystalline solid (90% yield). ^{1}H NMR (CD_2Cl_2, 400 MHz, 25 °C): δ 9.44 (s, 1H), 8.47 (s, 1H), 8.38 (d, J = 4.0 Hz, 4H), 8.13–8.09 (m, 4H), 8.00 (d, J = 8.8 Hz, 2H), 7.81–7.78 (m, 6H), 7.67 (d, J = 6.8 Hz, 4H), 7.56–7.52 (m, 4H), 7.47–7.43 (m, 2H), 6.69 (d, J = 8.8 Hz, 4H), 3.99 (br, 8H), 2.10 (br, 8H), 1.77–1.72 (m, 8H). ^{13}C{^{1}H} NMR (CD_2Cl_2, 100 MHz, 25 °C): δ 151.1, 146.4, 142.5, 133.4, 131.5, 130.93, 129.1, 127.8, 126.8, 125.9, 125.3, 123.4, 121.2, 117.6, 115.3, 94.20, 88.18, 85.43 (d, J_{Rh-C} = 123 Hz), 30.05 (two carbon atoms of the anthracene moieties were not observed due to poor solubility of the sample). Anal. Calcd for $C_{66}H_{56}B_2F_8N_6Rh_2 \cdot {}^1/_4CH_2Cl_2$: C, 59.20; H, 4.88; N, 6.46. Found: C, 59.62; H, 4.27; N, 6.30.

Synthesis of $Zn_2(1)Cl_4$ (2b). To a mixture of **1** (71.7 mg, 0.1 mmol) and $ZnCl_2$ (27.3 mg, 0.2 mmol) was added 5 mL of Et_2O, and the suspension was stirred overnight at ambient temperature. The product was collected by vacuum filtration and dried in vacuo (95% yield). ^{1}H NMR ($CDCl_3$, 400 MHz, 25 °C): δ 9.61 (s, 1H), 8.48 (s, 1H), 8.26 (d, J = 4.0 Hz, 4H), 8.02 (d, J = 4.0 Hz, 2H), 7.81 (d, J = 4.0 Hz, 2H), 7.63 (d, J = 4.0 Hz, 4H), 7.47–7.26 (m, 6H), 7.04 (d, J = 8.0 Hz, 4H), 6.98 (br, 2H), 6.94 (d, J = 8.0 Hz, 2H), 6.89–6.86 (m, 4H). ^{13}C{^{1}H} NMR ($CDCl_3$, 100 MHz, 25 °C): δ 157.7, 148.6, 145.1, 137.6, 133.1, 131.6, 131.4, 130.8, 128.9, 127.6, 126.6, 125.2, 124.1, 121.6, 120.0, 118.6, 117.2, 94.84, 87.99. Anal. Calcd for

dx.doi.org/10.1021/ic201757r | *Inorg. Chem.* 2012, 51, 7039–7049

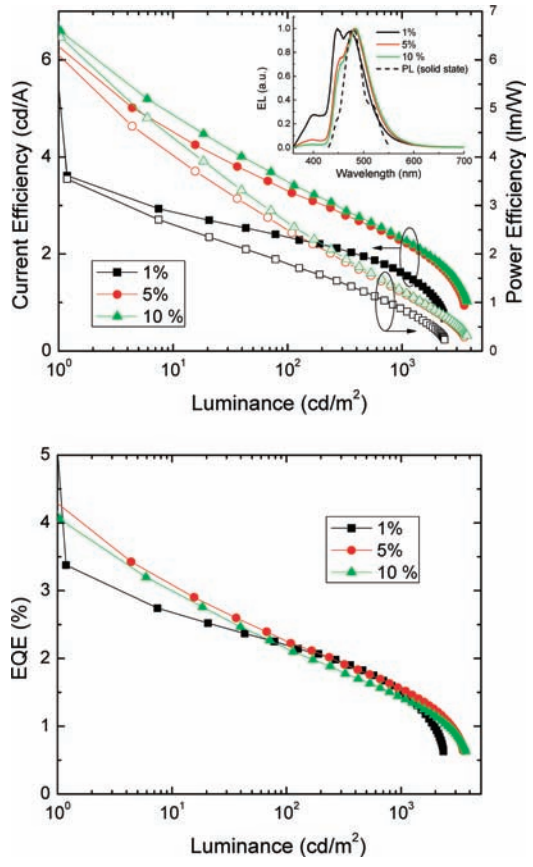

Figure 12. Current efficiency and power efficiency (top) and EQE of OLED devices with different doping concentrations of **1** in TPBi as EML (bottom). The inset gives the corresponding normalized EL spectra.

$C_{50}H_{32}N_6Zn_2Cl_4 \cdot {}^2/_3CH_2Cl_2$: C, 58.18; H, 3.21; N, 8.03. Found: C, 58.66; H, 2.68, N, 7.46.

Synthesis of Zn(1)(OTf)$_2$ (2c). To a solution of **1** (21.5 mg, 0.03 mmol, in 3 mL of CH_2Cl_2) was added a solution of $Zn(OTf)_2$ (11.2 mg, 0.03 mmol, in 5 mL of CH_3OH). The mixed solution was stirred for 2 h at ambient temperature. The solvent was then removed in vacuo, and the residue was recrytallized in dichloromethane/hexanes to afford the product as an orange-yellow crystalline solid (85% yield). ^{1}H NMR ($CDCl_3$ + CD_3OD, 400 MHz, 25 °C): δ 9.54 (s, 1H), 8.50 (s, 1H), 8.23 (d, J = 4.0 Hz, 4H), 8.05 (d, J = 4.0 Hz, 2H), 7.81 (dd, J = 6.8 Hz, J = 0.8 Hz, 2H), 7.65−7.63 (m, 8H), 7.49 (dd, J = 8.4 Hz, J = 6.8 Hz, 2H), 7.05−6.95 (m, 12H). ^{13}C{^{1}H} NMR ($CDCl_3$ + CD_3OD, 100 MHz, 25 °C): δ 158.7, 147.5, 143.7, 138.7, 132.9, 131.2, 131.0, 130.6, 128.8, 127.4, 125.8, 124.9, 124.7, 120.8, 120.4, 119.9 (q, J_{C-F} = 316 Hz), 119.2, 117.6, 93.87, 88.02. Anal. Calcd for $C_{50}H_{32}F_6N_6O_6S_2Zn \cdot CH_2Cl_2$: C, 54.66; H, 2.86; N, 7.22. Found: C, 54.64; H, 3.24; N, 7.16.

X-ray Diffraction Analyses. X-ray-quality crystals of **1** were obtained by top-layering a chloroform solution of **1** with hexanes, those of **2a** were obtained from a THF/DCM solution of **2a**, those of **2b** were obtained by vapor diffusion of pentane into a CH_2Cl_2 solution of **2b**, those of **2b′** were obtained from a THF/CH_3CN solution of **2b**, and those of **2c** were obtained by top-layering a DCM solution of **2c** with hexanes. All crystals were mounted on the tip of a MiTeGen MicroMount, and the single-crystal X-ray diffraction data were collected on a Bruker Kappa Apex II diffractometer. All data were collected with graphite-monochromated Mo Kα radiation (λ = 0.710 73 Å) at 150 K controlled by an Oxford Cryostream 700 series low-temperature system. The diffraction data were processed with the Bruker Apex 2 software package.[57] All structures were solved by direct methods and refined using SHELXTL V7.00.[58] Compound **1** crystallized in the monoclinic space group $P2_1/c$ with one molecule per asymmetric unit. **2a** crystallized in the triclinic space group $P\bar{1}$ with one molecule per asymmetric unit. **2b** crystallized in the orthorhombic space group *Pnna* with half a molecule per asymmetric unit. **2c** crystallized in the monoclinic space group $C2/c$ with half a molecule per asymmetric unit. Half a molecule of disordered dichloromethane was located in the crystal lattice of **2b**. The residual diffuse electron density of disordered and unidentified solvent molecules in the lattices of **2a**,**b**,**b′**,**c** were removed with the SQUEEZE function of PLATON,[59] and their contributions were not included in the formula. Elemental analysis of **2a** suggested that the removed electron densities may originate from THF molecules. All non-hydrogen atoms were refined anisotropically, except for the disordered portions. In all structures hydrogen atoms bonded to carbon atoms were included in calculated positions and treated as riding atoms. The crystallographic data are summarized in Table 1, while selected bond lengths and angles are given in Table 2.

Table 1. Crystallographic Data

	1	2a	2b·$^1/_2CH_2Cl_2$	2c
formula	$C_{50}H_{32}N_6$	$C_{67}H_{58}B_2Cl_2F_8N_6Rh_2$	$C_{50.5}H_{33}Cl_5N_6Zn_2$	$C_{52}H_{32}F_6N_6O_6S_2Zn$
fw	716.82	1397.53	1031.82	1080.33
T (K)	150(2)	150(2)	150(2)	150(2)
space group	$P2_1/c$	$P\bar{1}$	*Pnna*	$C2/c$
a (Å)	20.3101(9)	10.3248(5)	18.4630(10)	14.6487(4)
b (Å)	9.0336(3)	18.3669(9)	9.1420(5)	19.4576(6)
c (Å)	20.0894(9)	19.8936(11)	35.166(2)	16.5977(6)
α (deg)	90	109.469(2)	90	90
β (deg)	99.057(2)	100.819(2)	90	108.5820(10)
γ (deg)	90	102.057(2)	90	90
V (Å^3)	3639.9(3)	3340.1(3)	5935.6(6)	4484.2(2)
Z	4	2	4	4
D_c (g cm^{-3})	1.308	1.390	1.155	1.600
μ (mm^{-1})	0.078	0.640	1.067	0.728
no. of rflns collcd	30 520	55 337	27 067	20 002
no. of indep rflns	8292	15 138	6732	5151
GOF on F^2	0.958	1.028	0.947	1.052
R ($I > 2\sigma(I)$)	R1 = 0.0593, wR2 = 0.1087	R1 = 0.0504, wR2 = 0.1147	R1 = 0.0673, wR2 = 0.1528	R1 = 0.0512, wR2 = 0.1336
R (all data)	R1 = 0.1592, wR2 = 0.1389	R1 = 0.0848, wR2 = 0.1246	R1 = 0.1431, wR2 = 0.1767	R1 = 0.0751, wR2 = 0.1472

dx.doi.org/10.1021/ic201757r | *Inorg. Chem.* 2012, 51, 7039−7049

Table 2. Selected Bond Lengths (Å) and Angles (deg)

Ligand **1**			
C(1)−C(15)−C(16)	178.3(2)	C(34)−C(33)−C(11)	176.3(2)
C(15)−C(16)−C(17)	177.5(2)	C(33)−C(34)−C(35)	178.9(3)
Complex **2a**			
Rh(1)−N(2)	2.111(3)	Rh(1)−C(52)	2.109(4)
Rh(1)−N(3)	2.105(3)	Rh(1)−C(55)	2.126(4)
Rh(1)−C(51)	2.153(4)	Rh(1)−C(56)	2.120(4)
N(3)−Rh(1)−C(52)	90.80(13)	N(3)−Rh(1)−C(51)	95.02(13)
N(3)−Rh(1)−N(2)	84.87(10)	C(52)−Rh(1)−C(51)	37.82(16)
C(52)−Rh(1)−N(2)	152.41(15)	N(2)−Rh(1)−C(51)	169.69(14)
N(3)−Rh(1)−C(56)	161.2(2)	C(56)−Rh(1)−C(51)	80.34(16)
C(52)−Rh(1)−C(56)	96.28(17)	C(55)−Rh(1)−C(51)	90.08(16)
N(2)−Rh(1)−C(56)	96.45(14)	C(16)−C(15)−C(1)	175.8(4)
N(3)−Rh(1)−C(55)	161.32(19)	C(15)−C(16)−C(17)	174.6(4)
C(52)−Rh(1)−C(55)	82.24(16)	C(34)−C(33)−C(11)	174.7(4)
N(2)−Rh(1)−C(55)	93.28(14)	C(33)−C(34)−C(35)	176.1(4)
C(56)−Rh(1)−C(55)	37.5(2)		
Complex **2b**			
Zn(1)−N(2)	2.009(4)	Zn(1)−Cl(1)	2.2108(13)
Zn(1)−N(3)	2.014(4)	Zn(1)−Cl(2)	2.2141(13)
N(2)−Zn(1)−N(3)	89.12(15)	N(3)−Zn(1)−Cl(2)	112.29(11)
N(2)−Zn(1)−Cl(1)	113.52(11)	Cl(1)−Zn(1)−Cl(2)	114.40(5)
N(3)−Zn(1)−Cl(1)	111.54(11)	C(10)−C(9)−C(1)	177.2(6)
N(2)−Zn(1)−Cl(2)	113.42(11)	C(9)−C(10)−C(11)	174.6(6)
Complex **2c**[a]			
Zn(1)−N(1)	2.112(2)	Zn(1)−O(3)#1	2.136(2)
Zn(1)−N(1)#1	2.112(2)	Zn(1)−N(2)#1	2.140(3)
Zn(1)−O(3)	2.136(2)	Zn(1)−N(2)	2.140(3)
N(1)−Zn(1)−N(1)#1	98.62(14)	O(3)#1−Zn(1)−N(2)#1	89.81(10)
N(1)−Zn(1)−O(3)	87.39(10)	N(1)−Zn(1)−N(2)	95.24(10)
N(1)#1−Zn(1)−O(3)	171.53(10)	N(1)#1−Zn(1)−N(2)	83.72(10)
N(1)−Zn(1)−O(3)#1	171.53(10)	O(3)−Zn(1)−N(2)	89.81(10)
N(1)#1−Zn(1)−O(3)#1	87.39(10)	O(3)#1−Zn(1)−N(2)	91.34(10)
O(3)−Zn(1)−O(3)#1	87.30(14)	N(2)#1−Zn(1)−N(2)	178.41(14)
N(1)−Zn(1)−N(2)#1	83.72(10)	C(10)−C(9)−C(1)	175.6(3)
N(1)#1−Zn(1)−N(2)#1	95.23(10)	C(9)−C(10)−C(11)	171.1(3)
O(3)−Zn(1)−N(2)#1	91.34(10)		

[a]Symmetry transformation: (#1) $-x, y, -z + {}^{3}/_{2}$.

DFT Calculations. All calculations were performed using the Gaussian 09 software package[60] and B3LYP method.[61,62] All elements were treated with the 6-311++G** basis set. The structure of **1** was optimized in the gas phase with default convergence criteria. Self-consistent reaction field (SCRF) calculations using the PCM-UFF solvation model were performed on the optimized structures. THF was used in the PCM calculations. A vibrational frequency analysis was performed on the optimized structure to confirm that a local minimum is obtained.

Electrofluorescent Device Fabrication. All the devices were fabricated in a Kurt J. Lesker LUMINOS cluster tool with a base pressure of 10^{-8} Torr. Indium tin oxide (ITO) with a sheet resistance of 15 Ω/□ was commercially patterned on a glass substrate with a thickness of 1.1 mm. The ITO glass substrates were treated with a standard process: i.e., ultrasonic cleaning in Alconox, acetone, and methanol for 15 min, respectively, followed by a 15 min UV ozone treatment. After the UV ozone process, substrates were quickly loaded into the vacuum. MoO_3, CBP, EML, CBP, TPBi, LiF, and Al were sequentially deposited in different chambers without breaking the vacuum, where the EML is the emission layer that is a neat film of either **1** or **1** doped into different host molecules, i.e., α-NPD, CBP, and TPBi. The active area of all the devices was hence 2 mm.[28] Current−voltage (*IV*) characteristics were measured using an HP4140B pA meter. Luminance measurements were measured by a Minolta LS-110 luminance meter. EL spectra were measured by a USB 2000 miniature fiber optic spectrometer. All the measurements were conducted in ambient air. The EQE and power efficiency are calculated assuming a Lambertian emission pattern.

■ ASSOCIATED CONTENT

Ⓢ Supporting Information

CIF files giving crystallographic data for **1** and **2a**−**c** and figures and tables giving the crystal structure of **2b′**, details of the DFT calculations, the input structure of **1** in *Z* matrix for geometry optimization, and the atomic coordinates of optimized **1** in Cartesian coordinates. This material is available free of charge via the Internet at http://pubs.acs.org.

■ AUTHOR INFORMATION

Corresponding Author

*E-mail: dsong@chem.utoronto.ca.

Notes

The authors declare no competing financial interest.

■ ACKNOWLEDGMENTS

This research was supported by grants to D.S. and Z.-H.L. from the Natural Science and Engineering Research Council (NSERC) of Canada, the Canadian Foundation for Innovation, the Ontario Research Fund, and the ERA program of Ontario. R.T. is grateful for a postgraduate scholarship from the OGS program of Ontario. D.J.K. is grateful for financial support from the NSERC USRA program.

■ REFERENCES

(1) Accetta, A.; Corradini, R.; Marchelli, R. *Top. Curr. Chem.* **2011**, *300*, 175−216.
(2) Fabbrizzi, L.; Licchelli, M.; Rabaioli, G.; Taglietti, A. *Coord. Chem. Rev.* **2000**, *205*, 85−108.
(3) Gunnlaugsson, T.; Glynn, M.; Tocci, G. M.; Kruger, P. E.; Pfeffer, F. M. *Coord. Chem. Rev.* **2006**, *250*, 3094−3117.
(4) Martinez-Manez, R.; Sancenon, F. *Chem. Rev.* **2003**, *103*, 4419−4476.
(5) Prodi, L.; Bolletta, F.; Montalti, M.; Zaccheroni, N. *Coord. Chem. Rev.* **2000**, *205*, 59−83.
(6) Sagara, Y.; Kato, T. *Nat. Chem.* **2009**, *1*, 605−610.
(7) Sameni, S.; Jeunesse, C.; Matt, D.; Harrowfield, J. *Chem. Soc. Rev.* **2009**, *38*, 2117−2146.
(8) Haas, K. L.; Franz, K. J. *Chem. Rev.* **2009**, *109*, 4921−4960.
(9) Mewis, R. E.; Archibald, S. J. *Coord. Chem. Rev.* **2010**, *254*, 1686−1712.
(10) Montgomery, C. P.; Murray, B. S.; New, E. J.; Pal, R.; Parker, D. *Acc. Chem. Res.* **2009**, *42*, 925−937.
(11) Chen, L.; Lin, C.-C.; Yeh, C.-W.; Liu, R.-S. *Materials* **2010**, *3*, 2172−2195.
(12) Hudson, Z. M.; Wang, S. *Acc. Chem. Res.* **2009**, *42*, 1584−1596.
(13) Shimizu, M.; Hiyama, T. *Chem. Asian J.* **2010**, *5*, 1516−1531.
(14) Evans, R. C.; Douglas, P.; Winscom, C. J. *Coord. Chem. Rev.* **2006**, *250*, 2093−2126.

(15) Gareth Williams, J. A.; Develay, S.; Rochester, D. L.; Murphy, L. *Coord. Chem. Rev.* **2008**, *252*, 2596−2611.
(16) Holder, E.; Langeveld, B. M. W.; Schubert, U. S. *Adv. Mater. (Weinheim, Ger.)* **2005**, *17*, 1109−1121.
(17) Murphy, L.; Williams, J. A. G. *Top. Organomet. Chem.* **2010**, *28*, 75−111.
(18) Thompson, M. *MRS Bull.* **2007**, *32*, 694−701.
(19) Cottone, A., III; Scott, M. J. *Organometallics* **2000**, *19*, 5254−5256.
(20) Cottone, A., III; Scott, M. J. *Organometallics* **2002**, *21*, 3610−3627.
(21) De Felice, V.; Ruffo, F.; Tuzi, A. *Inorg. Chim. Acta* **1994**, *221*, 151−5.
(22) Fujihara, T.; Tsuge, K.; Sasaki, Y.; Kaminaga, Y.; Imamura, T. *Inorg. Chem.* **2002**, *41*, 1170−1176.
(23) Guilard, R.; Gros, C. P.; Barbe, J.-M.; Espinosa, E.; Jerome, F.; Tabard, A.; Latour, J.-M.; Shao, J.; Ou, Z.; Kadish, K. M. *Inorg. Chem.* **2004**, *43*, 7441−7455.
(24) Guilard, R.; Jerome, F.; Barbe, J.-M.; Gros, C. P.; Ou, Z.; Shao, J.; Fischer, J.; Weiss, R.; Kadish, K. M. *Inorg. Chem.* **2001**, *40*, 4856−4865.
(25) Harvey, P. D.; Proulx, N.; Martin, G.; Drouin, M.; Nurco, D. J.; Smith, K. M.; Bolze, F.; Gros, C. P.; Guilard, R. *Inorg. Chem.* **2001**, *40*, 4134−4142.
(26) Jerome, F.; Barbe, J.-M.; Gros, C. P.; Guilard, R.; Fischer, J.; Weiss, R. *New J. Chem.* **2001**, *25*, 93−101.
(27) Lachkar, M.; Tabard, A.; Brandes, S.; Guilard, R.; Atmani, A.; De Cian, A.; Fischer, J.; Weiss, R. *Inorg. Chem.* **1997**, *36*, 4141−4146.
(28) Ojida, A.; Mito-oka, Y.; Sada, K.; Hamachi, I. *J. Am. Chem. Soc.* **2004**, *126*, 2454−2463.
(29) Sarkar, S.; McGowan, K. P.; Culver, J. A.; Carlson, A. R.; Koller, J.; Peloquin, A. J.; Veige, M. K.; Abboud, K. A.; Veige, A. S. *Inorg. Chem.* **2010**, *49*, 5143−5156.
(30) Yoshinori, S.; Sawada, N.; Tadokoro, M. *Chem. Lett.* **1994**, 1713−16.
(31) Weng, Y. -Q; Yue, F.; Zhong, Y. -R; Ye, B. -H. *Inorg. Chem.* **2007**, *46*, 7749.
(32) Mooibroek, T. J.; Aromi, G.; Quesada, M.; Roubeau, O.; Gamez, P.; DeBeer George, S.; van Slageren, J.; Yasin, S.; Ruiz, E.; Reedijk, J. *Inorg. Chem.* **2009**, *48*, 10643.
(33) Pang, J.; Tao, Y.; Yang, X.-P.; D'Iorio, M.; Wang, S. *J. Mater. Chem.* **2002**, *12*, 206.
(34) Kang, Y.; Lee, J.; Song, D.; Wang, S. *Dalton Trans.* **2003**, 3493.
(35) Liu, Q.; Jia, W.; Wu, G.; Wang, S. *Organometallics* **2003**, *22*, 3781.
(36) Lee, J.; Liu, Q.; Motala, M.; Dane, J.; Gao, J.; Kang, Y.; Wang, S. *Chem. Mater.* **2004**, *16*, 1869.
(37) Bai, D.; Wang, S. *Organometallics* **2006**, *25*, 1517.
(38) Martic, S.; Wu, G.; Wang, S. *Inorg. Chem.* **2008**, *47*, 8315.
(39) Wong, E.; Li, J.; Seward, C.; Wang, S. *Dalton Trans.* **2009**, 1776.
(40) Sonogashira, K. *J. Organomet. Chem.* **2002**, *653*, 46.
(41) Hlavinka, M. L.; McNevin, M. J.; Shoemaker, R.; Hagadorn, J. R. *Inorg. Chem.* **2006**, *45*, 1815.
(42) Foxon, S.; Xu, J.; Turba, S.; Leibold, M.; Hampel, F.; Heinemann, F. W.; Walter, O.; Wuertele, C.; Holthausen, M.; Schindler, S. *Eur. J. Inorg. Chem.* **2007**, 429.
(43) (a) Kang, Y.; Seward, C.; Song, D.; Wang, S. *Inorg. Chem.* **2003**, *42*, 2789−2797. (b) Bai, D.-R.; Wang, S. *Organometallics* **2004**, *23*, 5958−5966. (c) Gupta, G.; Gloria, S.; Therrien, B.; Das, B.; Rao, K. M. *J. Organomet. Chem.* **2011**, *696*, 702−708.
(44) (a) Ghosh, S.; Gole, B.; Bar, A. K.; Mukherjee, P. S. *Organometallics* **2009**, *28*, 4288−4296. (b) Augouy, L.; Huby, N.; Hirsch, L.; van der Lee, A.; Gerbier, P. *New J. Chem.* **2009**, *33*, 1290−1300.
(45) Dahl, K.; Biswas, R.; Ito, N.; Maroncelli, M. *J. Phys. Chem. B* **2005**, *109*, 1563−1585.
(46) Zhao, S.-B.; Wucher, P.; Hudson, Z. M.; McCormick, T. M.; Liu, X.-Y.; Wang, S.; Feng, X.-D.; Lu, Z.-H. *Organometallics* **2008**, *27*, 6446−6456.
(47) The dielectric constants of dichloromethane and THF at room temperature are 9.1 and 7.5, respectively, much smaller than that of methanol (33). For a comprehensive list of dielectric constants of solvents, see: Haynes, W. M. *CRC Handbook of Chemistry and Physics*, 91st ed.; CRC Press: Boulder, CO, 2010.
(48) Fayed, T. A.; El-Morsi, M. A.; El-Nahass, M. N. *J. Photochem. Photobiol., A* **2011**, *224*, 38−45.
(49) Wang, Z. B.; Helander, M. G.; Qiu, J.; Liu, Z. W.; Greiner, M. T.; Lu, Z. H. *J. Appl. Phys.* **2010**, *108*, 024510.
(50) Wang, Z. B.; Helander, M. G.; Qiu, J.; Puzzo, D. P.; Greiner, M. T.; Liu, Z. W.; Lu, Z. H. *Appl. Phys. Lett.* **2011**, *98*, 073310.
(51) Wang, Z. B.; Helander, M. G.; Liu, Z. W.; Greiner, M. T.; Qiu, J.; Lu, Z. H. *Appl. Phys. Lett.* **2010**, *96*, 043303.
(52) Tang, C. W.; VanSlyke, S. A.; Chen, C. H. *J. Appl. Phys.* **1989**, *65*, 3610.
(53) Wen, S.-W.; Lee, M.-T.; Chen, C. H. *J. Display Technol.* **2005**, *1*, 90.
(54) Perez-Trujillo, M.; Maestre, I.; Jaime, C.; Alvarez-Larena, A.; Piniella, J. F.; Virgili, A. *Tetrahedron: Asymmetry* **2005**, *18*, 3084.
(55) Kang, Y.; Seward, C.; Song, D.; Wang, S. *Inorg. Chem.* **2003**, *8*, 2789.
(56) Rodman, G. S.; Mann, K. R. *Inorg. Chem.* **1988**, *19*, 3338.
(57) *Apex 2 Software Package*; Bruker AXS Inc., 2008.
(58) Sheldrick, G. M. *Acta Crystallogr., Sect. A: Found. Crystallogr.* **2008**, *64*, 112.
(59) Spek, A. L. J. *Appl. Crystallogr.* **2003**, *36*, 7.
(60) Frisch, M. J.; Trucks, G. W.; Schlegel, H. B.; Scuseria, G. E.; Robb, M. A.; Cheeseman, J. R.; Scalmani, G.; Barone, V.; Mennucci, B.; Petersson, G. A.; Nakatsuji, H.; Caricato, M.; Li, X.; Hratchian, H. P.; Izmaylov, A. F.; Bloino, J.; Zheng, G.; Sonnenberg, J. L.; Hada, M.; Ehara, M.; Toyota, K.; Fukuda, R.; Hasegawa, J.; Ishida, M.; Nakajima, T.; Honda, Y.; Kitao, O.; Nakai, H.; Vreven, T.; Montgomery, J. A., Jr.; Peralta, J. E.; Ogliaro, F.; Bearpark, M.; Heyd, J. J.; Brothers, E.; Kudin, K. N.; Staroverov, V. N.; Keith, T.; Kobayashi, R.; Normand, J.; Raghavachari, K.; Rendell, A.; Burant, J. C.; Iyengar, S. S.; Tomasi, J.; Cossi, M.; Rega, N.; Millam, J. M.; Klene, M.; Knox, J. E.; Cross, J. B.; Bakken, V.; Adamo, C.; Jaramillo, J.; Gomperts, R.; Stratmann, R. E.; Yazyev, O.; Austin, A. J.; Cammi, R.; Pomelli, C.; Ochterski, J. W.; Martin, R. L.; Morokuma, K.; Zakrzewski, V. G.; Voth, G. A.; Salvador, P.; Dannenberg, J. J.; Dapprich, S.; Daniels, A. D.; Farkas, O.; Foresman, J. B.; Ortiz, J. V.; Cioslowski, J.; Fox, D. J. *Gaussian 09, Revision B.01*; Gaussian, Inc., Wallingford, CT, 2010.
(61) Becke, A. D. *J. Chem. Phys.* **1993**, *98*, 5648.
(62) Lee, C.; Yang, W.; Parr, R. G. *Phys. Rev. B* **1988**, *37*, 785.